UV/Solar Photo-degradation of furaltadone in homogeneous and heterogeneous phases: intensification with persulfate

Antonio Durán[1*], José María Montegudo[1], D. Castillo[1], Antonio J. Expósito[2]

[1]Department of Chemical Engineering, Grupo IMAES. ETSII, Instituto de Investigaciones Energéticas y Aplicaciones Industriales (INEI). Universidad de Castilla-La Mancha, Avda. Camilo José Cela 3, 13071 Ciudad Real (Spain). Phone: 0034 926295300, ext: 3814. email: antonio.duran@uclm.es

[2] Department of Chemical Engineering, University of Bath, Claverton Down, Bath BA2 7AY, UK.

* To whom correspondence should be addressed

Graphical Abstracts

Click here to access/download;Graphical Abstracts;Graphical abstract.docx

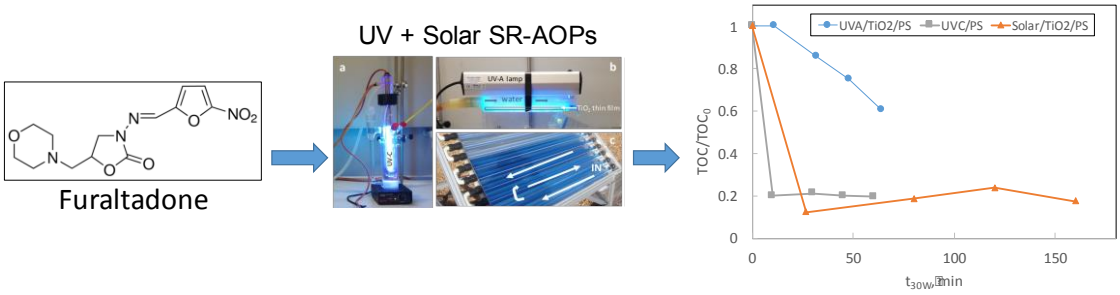

HIGHLIGHTS

- A complete study on FTD mineralization in homogeneous and heterogenous phase.
- Batch, heterogeneous thin film and CPC reactors were used.
- In homogeneous phase, the UV/PS system yields 80% of mineralization in 30 min.
- A dual mineralization mechanism based on sulfate radicals and holes is proposed
- The Solar/TiO_2/PS process has the lower operation costs

UV/Solar Photo-degradation of furaltadone in homogeneous and heterogeneous phases: intensification with persulfate

Antonio Durán[1*], José María Montegudo[1], D. Castillo[1], Antonio J. Expósito[2]

[1]Department of Chemical Engineering, Grupo IMAES. ETSII, Instituto de Investigaciones Energéticas y Aplicaciones Industriales (INEI). Universidad de Castilla-La Mancha, Avda. Camilo José Cela 3, 13071 Ciudad Real (Spain). Phone: 0034 926295300, ext: 3814. email: antonio.duran@uclm.es

[2] Department of Chemical Engineering, University of Bath, Claverton Down, Bath BA2 7AY, UK.

* To whom correspondence should be addressed

ABSTRACT

Previous studies on removal of the pharmaceutical drug Furaltadone (FTD) in water have not shown to be totally efficient or are very expensive. In this study, sulfate radicals derived from persulfate anions activated with different irradiation sources (UVA, UVC and solar light) and combined with H_2O_2 and/or TiO_2 have been tested in homogeneous and heterogeneous phases under different operation modes and reaction systems.

In homogeneous phase, UV produces a slow mineralization (k= 0.0013 min^{-1}). The combined processes are faster ($k_{UV/H2O2}$= 0.0185 min^{-1}, $k_{UV/PS}$ = 0.0206 min^{-1}) with the best performance for the UV/PS system yielding nearly 80% of mineralization in half an hour. The overall process (UV/H_2O_2/PS) does not show synergy and mineralization is even slower ($k_{UV/H2O2/PS}$ = 0.015 min^{-1}) due to the production of a high amount of radicals favouring unproductive reactions (scavenger effect). A mineralization mechanism is proposed involving formation of 5hydroxymethylene-2(5H)-furanone and NO as the main intermediates.

In heterogeneous phase (UVA/TiO_2/PS), the holes play an important role changing the mineralization mechanism. The main intermediates formed were $C_{12}H_{17}N_4O_4$ and $C_{11}H_{14}N_3O_4$, which rapidly were degraded to form $C_8H_{15}O_3N_3$, $C_4H_{10}NO$ and $C_5H_{10}NO$.

An economic study of operation costs has been made for selected processes: UVC/PS, UVA/TiO_2/PS and Solar/TiO_2/PS. The Solar/TiO_2/PS process has the lowest operation costs due to the use of solar energy. However, it would need an additional stage to recover the catalyst.

Finally, a loss of 27% in efficiency during mineralization was found after 5 cycles, but the catalyst recovers its initial performance after regeneration at 500 ºC.

Keywords: mechanism; persulfate, solar energy; titanium dioxide; water treatment

1. INTRODUCTION

Antibiotic is a revolutionary discovery for human healing, but is also used for other purposes such as agriculture and animal farming. Despite their great advantages, antibiotics have also hazards associated with pollution derived from a partial degradation into the environment. Due to new techniques, antibiotics have been detected in hospitals, dairy, and agriculture (Yu et al., 2013) and in WWTPs, where they are only partially removed (Bao et al., 2021).

Among them, furaltadone (FTD) is a highly effective pharmaceutical drug derivative of nitrofurans (NFs) used as an antibacterial agent in humans and animals, especially in birds. As negative effects, it can be highlighted that FTD inhibits nucleic acid synthesis, having toxic and allergic effects in hypersensitive people.

However, some countries still dispense nitrofurans to treat animal diseases (Nakamura et al., 2008, Balamurugan et al, 2021). Thus, residues of NFs are detected in many cultured animals (Chu and Lopez, 2007; Hu et al., 2007). For example, nitrofuran metabolites can be present in eggs and chicken muscles after the administration of furaltadone antibiotics (Finzi et al., 2005; Marques-Violante et al., 2018). Moreover, due to its low biodegradation, FTD, NFs and derivatives evacuated by animals may contaminate water environments that can be used for animal culture or agriculture, or even as a potable water source with the consequent toxic effects (Samuelsen et al., 1991; Nakamura et al., 2008).

There is an urgent need for removing FTD in order to protect the environment and preserve the aquatic ecosystem. To date, previous studies on the removal of FTD in water with advanced oxidation processes in homogeneous phase have not shown to be totally efficient or are very expensive (Edhlund et al., 2006; Bao et al., 2008). Pacholak et al.

(2020) reported 87.3% of removal of FTD with activated sludge in a long process (72h), but they do not mention mineralization, so that intermediates may be still present in water.

Recently, sulfate-radical-based AOPs are becoming important because of the high reactivity of sulfate radicals anion ($E° = 2.6$ V) with many compounds (Khan et al., 2014). Sulfate radicals could be derived from persulfate anions activated with heat energy, UV light, or electron transfer of transition metal ions. In this study, the use of persulfate (PS) activated with UVC light combined with H_2O_2 in homogeneous phase has been tested.

On the other hand, heterogeneous photocatalysis with TiO_2 is a widely used technique to degrade pollutants in water (Awfa et al., 2018; Kaman et al., 2019). TiO_2 can generate reactive oxidation species (ROS) such as hydroxyl, superoxide and perhydroxyl anion radicals that can react with contaminants (Farouk et al, 2016). However, the use of this photocatalyst has some drawbacks: the difficulty of scaling up the processes and the presence of the semiconductor suspended in the water (Domínguez et al., 2015). This last disadvantage can be solved if the titanium dioxide is immobilized. A wide range of immobilization techniques allow the regeneration of TiO_2 easily (Durán et al., 2018), but even so immobilization of the catalyst decreases the efficiency of matter transfer (Boiarkina et al., 2013). Thus, in order to improve the photodegradation yield in TiO_2 photocatalysis, it is possible to prevent electron-hole pair recombination adding electron acceptors such as sodium persulfate (PS) or hydrogen peroxide (Mills and Valenzuela, 2004; Yu et al., 2010: Saien et al., 2011; Jiménez-Tototzintle et al., 2015; Bekkouche, et al., 2017). In this work, a UVA/TiO_2/PS system has been used in an open reactor where the catalyst is supported as a thin film on a glass surface.

To sum it up, the aim of this paper is to explore the photodegradation and mineralization of furaltadone in water both in homogenous and heterogeneous systems under UVC and

UVA radiation respectively with different reaction systems and operation modes. The intensification of mineralization with PS is also explained. In addition, a solar-driven reaction was also conducted to reduce costs associated with the use of artificial lamps (an economic study of operation costs is included).

Finally, different mineralization routes have been proposed according to intermediates evolution and taking into account the role of the different radicals involved in each process.

2. MATERIALS AND METHODS

2.1. Materials

Furaltadone (99%) and 30% hydrogen peroxide (H_2O_2) were acquired from Sigma-Aldrich and Fisher Scientific respectively and were used without further purification. Sodium persulfate ($Na_2S_2O_8$, 98%) was obtained from Panreac. Technical grade TiO_2 P-25 from Degussa (anatase/rutile=3.6/1 wt, surface area 56 m^2 g^{-1}) was used as photocatalyst. Characterization of TiO_2 samples by X-ray diffraction (XRD), Raman spectroscopy, Transmission electron microscopy (TEM), Z-potential measurements, BET analysis and ultraviolet–Visible (UV–Vis) reflectance spectra were previously published by the authors (Monteagudo et al., 2020).

For the experimental runs focused on the evaluation of the kinetic mechanism, different radical scavengers were added to the system: p-benzoquinone, methanol and glycerol were supplied by Sigma-Aldrich.

2.2. Analytical methods

Furaltadone was quantified using a Gilson 231 XL high-performance liquid chromatography with UV detection (HPLC) and an Eclipse XDB-C18 column. Total

organic carbon was measured with a TOC analyzer (Shimadzu TOC-5000A). Determination of hydroxyl radicals was made with a RF 6000 spectro-fluorophotometer (Shimadzu) after reaction with disodium salt of terephthalic acid (NaTA) (Durán et al., 2018). Intermediates were analyzed with a QTOF-UHPLC (more information is given in Supplementary Material, text S1).

The residual $S_2O_8^{2-}$ concentration was analyzed by measuring the iodide produced after adding sodium carbonate and potassium iodide to the samples according to the method described by Liang et al. (2008).

Toxicity was evaluated by determining the inhibitory effect of water samples on the light emission of *Vibrio fischeri* (Luminescent bacteria test; 30 min incubation time) using a luminometer (Optocomp BG-1, Gomensoro) according to ISO 11,348-3:1998.

2.3. Reactor systems

Table 1 summarizes the different experimental reaction systems used in this work.

Table 1. Degradation of furaltadone with persulfate (activated with UV light) under different reaction systems

Process	Operation mode	Reactor system	Radiation	Tests
HOMOGENEOUS	Discontinuous	Batch (0.4 L)	UVC 15 W (254 nm)	H_2O_2 PS UVC UVC/H_2O_2 UVC/PS UVC/H_2O_2/PS Scavengers
HETEROGENEOUS	Continuous with recirculation	Thin film (total vol= 0.4 L)	UVA 8x2 W (>350 nm)	UVA UVA/TiO_2 UVA/TiO_2/PS UVA/TiO_2/H_2O_2 UVA/TiO_2/H_2O_2/PS Scavengers
	Continuous with recirculation	CPC (2 L)	Solar (UVA = 30W/m^2)	Solar/TiO_2/PS

2.3.1. Homogeneous photo-reactor

All experiments were carried out in triplicate in a 400-mL stirred photoreactor with an external jacket connected to a thermostatic bath to maintain a constant temperature (Figure 1a). A Heraeus TNN15/32 UV Hg immersible lamp with a nominal output of 15 W emitting at λ = 254 nm was used to irradiate the solutions. More details can be found in literature (Monteagudo et al., 2016)

2.3.2. Heterogeneous Thin-film photo-reactor

An open glass reactor (Figure 1b) was irradiated with a UVA lamp (> 350 nm, 2x8W, Vilber BVL-208-BL). A flow rate of 42 L/h of wastewater containing furaltadone (10 ppm, whole volume of 0.4 L) was fed to the system. TiO_2 was immobilized on the outer surface of a flat glass plate (25.4 x 7.7 cm) using a dip-coating method (Van Grieken et al., 2009). The detailed procedure can be found in the Supplementary Material (Text S2).

2.3.3. Solar CPC reactor

The experimental set-up is shown in Figure 1c and is described in detail in the literature (Monteagudo et al., 2010). It consisted of a CPC solar reactor (irradiated volume 2 L; Surface = 0.25 m^2). FTD is added to water in a 1.5 L stirred tank and is later fed to the reactor using a centrifugal pump (flow rate = 30 L min^{-1}).

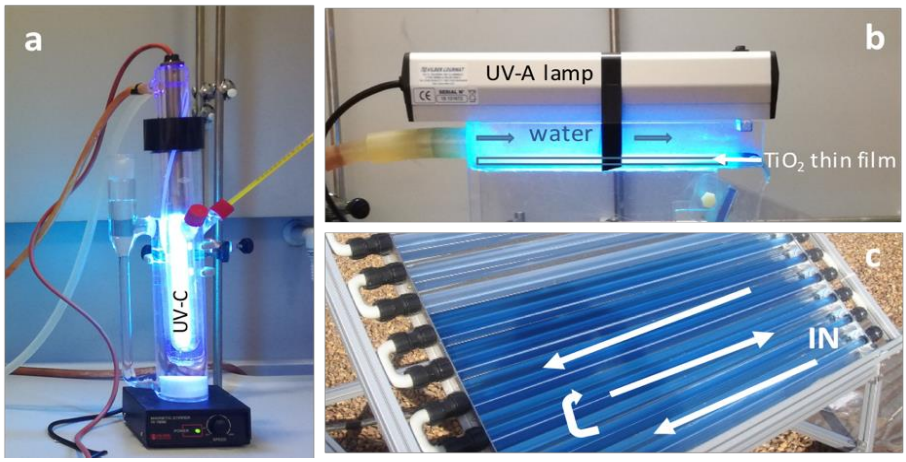

Figure 1. Detail of the reactor systems. a) Homogeneous batch reactor (UVC), b) Heterogeneous thin film reactor (UVA), c) Solar CPC reactor

3. RESULTS AND DISCUSSION

3.1. Homogeneous processes (Batch reactor with UVC radiation)

Initial pH was fitted in 4 as selected in previous works (Monteagudo et al., 2020b) and in order to compare results with heterogeneous photocatalysis (section 3.2). The concentration of PS was previously optimized to 2 mM. Under these conditions, H_2O_2 or PS alone produces less than 10% of degradation. However, the processes involving UVC light allow the complete removal of FTD in less than 5 minutes since this pollutant can absorb at 254 nm (as shown in the spectra in Figure S1, Supplementary Material).

Figure S1, Supplementary Material

Nevertheless, intermediates still remain in the solution, so mineralization must be studied to select a proper optimum process. As shown in Figure 2a, UVC alone produces a low mineralization degree (with a first-order rate constant k_{UVC} = 0.0013 min^{-1}). The combined processes are faster ($k_{UVC/H2O2}$= 0.0185 min^{-1}, $k_{UVC/PS}$ = 0.0206 min^{-1}) with the best performance for the UVC/PS system yielding nearly 80% of mineralization in half an hour. The overall process (UVC/H_2O_2/PS) does not show synergy exhibiting even slower kinetics ($k_{UV/H2O2/PS}$ = 0.015 min^{-1}). The reason for this behaviour can be found in the reactions involved. When both PS and H_2O_2 are irradiated with UVC, both sulfate and hydroxyl radicals are produced. In addition, some extra hydroxyl radicals can be formed via equation (1). However, this process is pH-dependent (Norzaee et al., 2017) so the $SO_4^{\bullet-}$ radical is dominant under low pHs.

$$SO_4^{-\bullet} + OH^- \rightarrow SO_4^{-2} + HO^\bullet \qquad (1)$$

However, the overall process (UVC/H_2O_2/PS) produces such an amount of radicals (Figure 2b) that favours the well-known scavenger effect where H_2O_2 is consumed in unproductive reactions. Thus, the UVC/PS process was selected for the rest of the study.

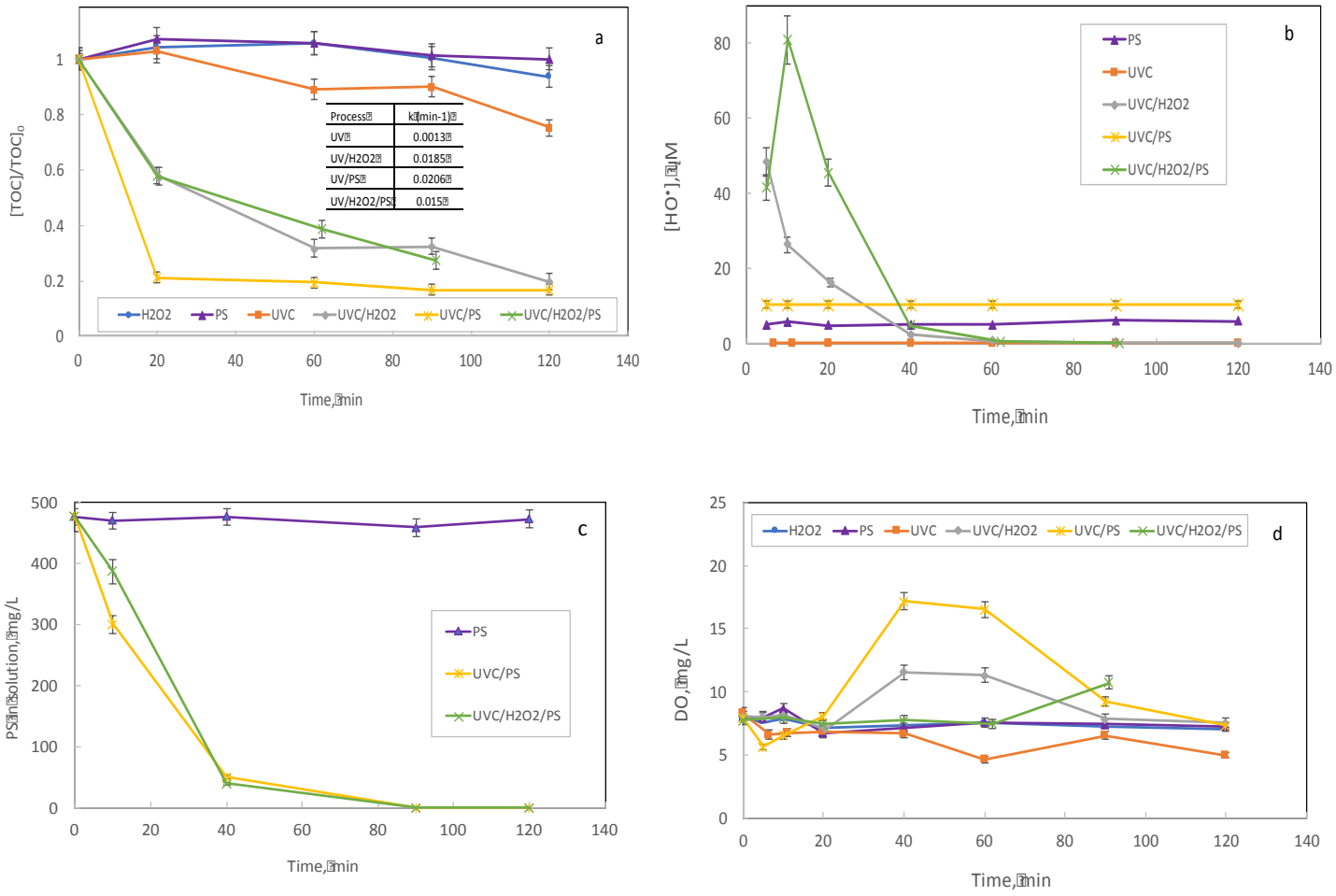

Fig. 2. Mineralization of FTD under different processes. a) TOC removal; b) Evolution of hydroxyl radicals; c) Evolution of PS; d) Dissolved oxygen. (Conditions: [FTD] = 0.03 mM; T = 30ºC; pH = 3.5; [PS]=2 mM; [H_2O_2]=5 mM)

Degradation of FTD under the selected UVC/PS process: study with radical scavengers and mineralization mechanism

It can be observed in Figure 2c that PS is quickly consumed during the first 40 minutes in the UVC–activated processes, being completely spent after 90 minutes (when mineralization reaches 80%). On the other hand, the maximum concentration of O_2 is found when operating under the selected UVC/PS system (Figure 2d), since the excess sulfate radicals react with HO^* according to:

$$SO_4^{-\bullet} + HO^{\bullet} \rightarrow HSO_4^{-} + 0.5\,O_2 \qquad (2)$$

In addition, the degradation of FTD in this process results in acid production (pH decrease) as shown in Figure 3. The S-shape curve with the increase in $[H^+]$ after FTD removal (3 minutes) implies that it comes from intermediates (Edhlund et al., 2006), as will be proposed below in the mineralization mechanism.

In order to determine the role of the main radical oxidative species (ROS) present in the reactor, additional tests with radical scavengers were performed. Methyl alcohol is used to inhibit both $HO^{\bullet}$ and $SO_4^{\bullet-}$ since it reacts at similar rates with both ROS (Anipsitakis and Dionysiou, 2004; Matta et al., 2011). On the other hand, 1,4-benzoquinone reacts with sulfate radicals (formed when PS is activated in the presence of UVC light, see Figure S2) and can be used to scavenge these radicals. Although methyl alcohol partially inhibits degradation (Figure 3), the formation of $HO^{\bullet}$ from sulfate radicals at acidic pH must be low according to equation (1) with an irrelevant effect on the process. Effectively, results demonstrate that the degradation of FTD is mainly inhibited by p-benzoquinone, pointing to the main role of sulfate radicals.

Figure S2, Supplementary Material

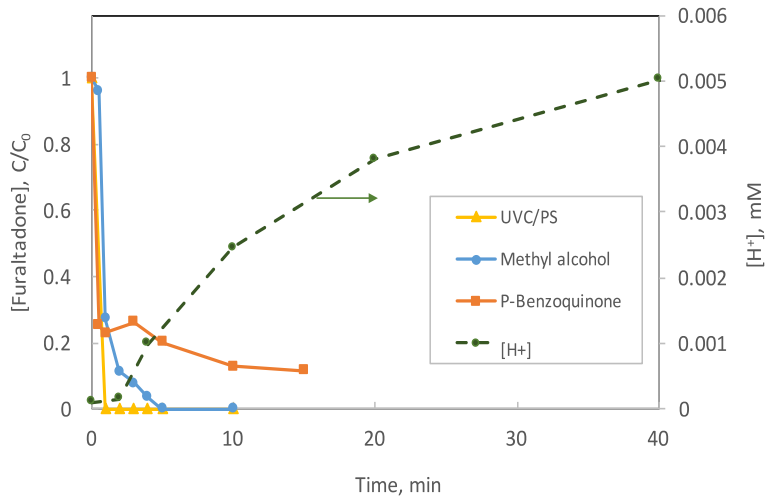

Figure 3. Degradation of FTD under the effect of different scavenger agents in the UVC/PS process. Evolution of $[H^+]$ without scavengers. (Conditions: [FTD] = 0.03 mM; T = 30ºC; [PS]=2 mM).

On the other hand, Figure S3 shows the main intermediate products found by LC-MS during the degradation of FTD in the UVC/PS process. According to these findings, a possible degradation mechanism has been proposed (route 1 in Figure 4). It can be assumed that FTD is initially broken to form $C_8H_{13}O_3N_3$ and 5-nitro-2-furaldehyde ($C_5H_3O_4N$). The latter degrades though the formation of 5hydroxymethylene-2(5H)-furanone and NO. Nitric oxide can be oxidized by dissolved oxygen yielding nitrous acid (HNO_2) that decreases pH as previously shown in Figure 3. Finally, the degradation continues until the formation of C_2-C_6 organic acids and the total mineralization to CO_2.

Figure S3, supplementary material

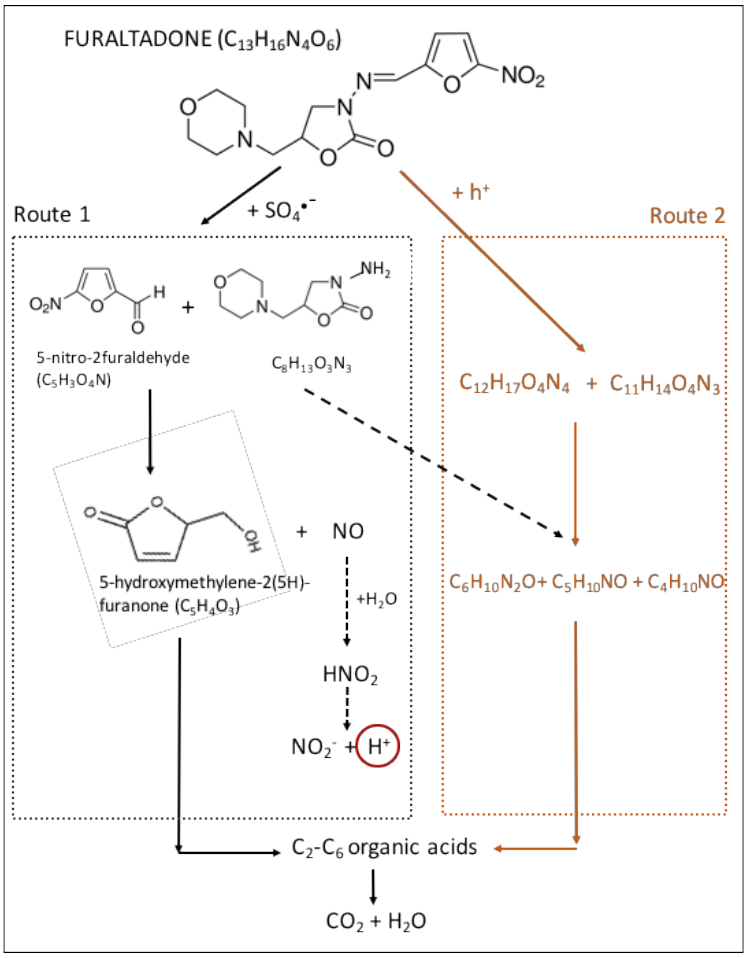

Figure 4. Proposed mineralization mechanism of FTD, based on intermediates of reaction for the UVC/PS process (route 1) and UVC/TiO_2/PS (route 2).

3.2. Heterogeneous processes

The degradation of FTD in heterogeneous phase was performed using TiO_2 as photo-catalyst. Previously, adsorption of FTD by TiO_2 was discarded as a main removal process, since experimental tests showed less than 10% was retained at different pHs (Figure S4, Supplementary Material)

Figure S4, Supplementary Material

3.2.1. Thin-film reactor (with UVA radiation)

A UVA lamp emitting at 365 nm was used to promote the formation of photogenerated charge carriers, hole (h_{VB}^{+}) and electron (e_{CB}^{-}) in the valence and conduction bands, respectively (Fraouk et al., 2016):

$$TiO_2 + h\upsilon \rightarrow TiO_2(e_{BC}^{-} + h_{BV}^{+}) \quad (3)$$

$$TiO_2(h_{BV}^{+}) + H_2O \rightarrow TiO_2 + HO_{ads}^{\bullet} + H^{+} \quad (4)$$

$$TiO_2(h_{BV}^{+}) + OH^{-} \rightarrow TiO_2 + HO_{ads}^{\bullet} \quad (5)$$

$TiO_2(h_{VB}^{+})$ symbolizes the surface of TiO_2 with holes and $HO_{ads}^{\bullet}$, the hydroxyl radical adsorbed on that surface.

In addition, other reactions radicals can be formed on the surface of the semiconductor (equations 6, 7) and the pollutant can be degraded directly on the surface of the TiO_2 particle (equation 8):

$$TiO_2(e_{BC}^{-}) + O_2 \rightarrow TiO_2 + O_2^{\bullet -} \quad (6)$$

$$O_2^{\bullet -} + H^{+} \rightarrow HO_2^{\bullet} \quad (7)$$

$$Pollutant + h_{VB}^{+} \rightarrow Products \quad (8)$$

On the other hand, as commented above, sodium persulfate was added to the system in this case as an electron acceptor to prevent electron-hole pair recombination and improve the degradation efficiency (Mills and Valenzuela, 2004).

Figure 5 shows the degradation and mineralization of FTD under individual and combined heterogeneous processes. UVA radiation alone is capable to produce 95% of degradation in 120 minutes (k= 0.227 min^{-1}). This is due to the high absorption of FTD in the UVA region where the lamp emits (> 365nm) as shown in the spectra in Figure S1). Other processes tested (UVA/TiO_2 and UVA/TiO_2/H_2O_2 with [TiO_2] = 0.36 mg/cm^2) allow a complete degradation of FTD after 2 hours. However, the most efficient processes imply the presence of persulfate. The overall combined process (UVA/TiO_2/H_2O_2/PS) is again less efficient. The use of a higher loading ([TiO_2] = 0.64 mg/cm^2, UVA/TiO_2*/H_2O_2) does not improve results.

Regarding mineralization (Figure 6b), 38% is reached after 2 hours and 48% in 3 hours when the UVA/TiO_2/PS process is operated. The equivalent process in homogeneous phase (for the same reactor volume and similar power) with UVC radiation (UVC/PS) achieved 80% of mineralization in just 20 minutes. Thus, in order to make more efficient the heterogeneous process an environmental alternative consisting of obtaining UVA radiation directly from the Sun using concentrated solar energy was tested (as will be studied below in section 3.2.3).

i) Study with radical oxidative specie (ROS) scavengers and mechanism

A new set of experiments was performed to study the role of the different ROS present in the system. Again, methyl alcohol is used to inhibit both $HO^{\bullet}$ and $SO_4^{\bullet-}$ and now glycerol was used here as a selective hole scavenger (Ibadurrohman and Hellgardt, 2014). Results (shown in Figure S5 in Supplementary Material) demonstrate that methanol does not affect the degradation of FTD, indicating the secondary role of both $HO^{\bullet}$ and $SO_4^{\bullet-}$ radicals. On the contrary, glycerol has a significant effect, which is indicative of the main role of holes in the process.

Figure S5, Supplementary Material

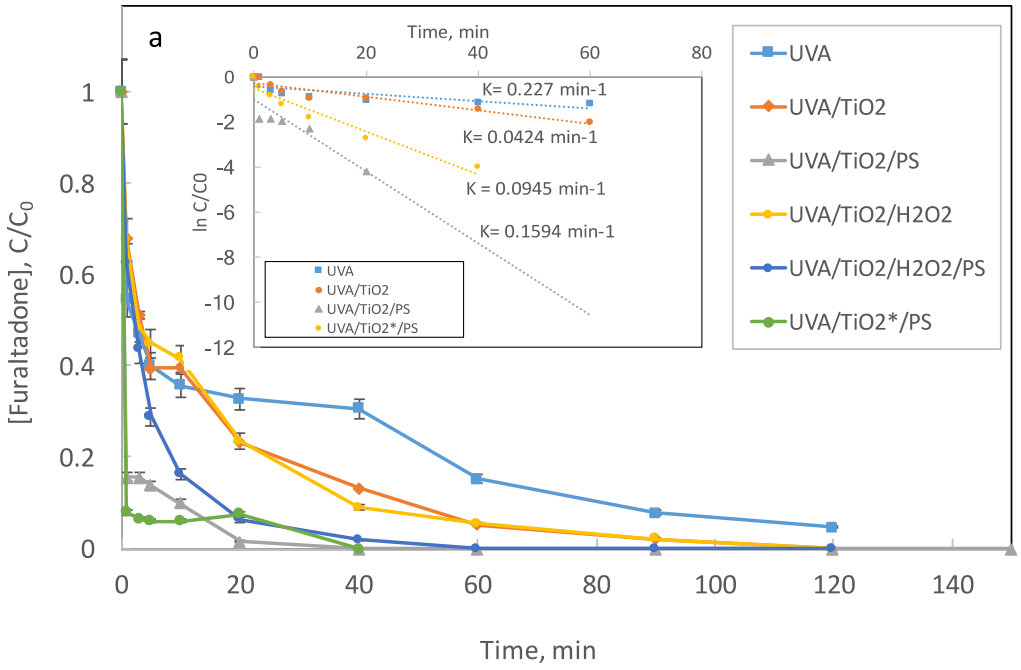

288

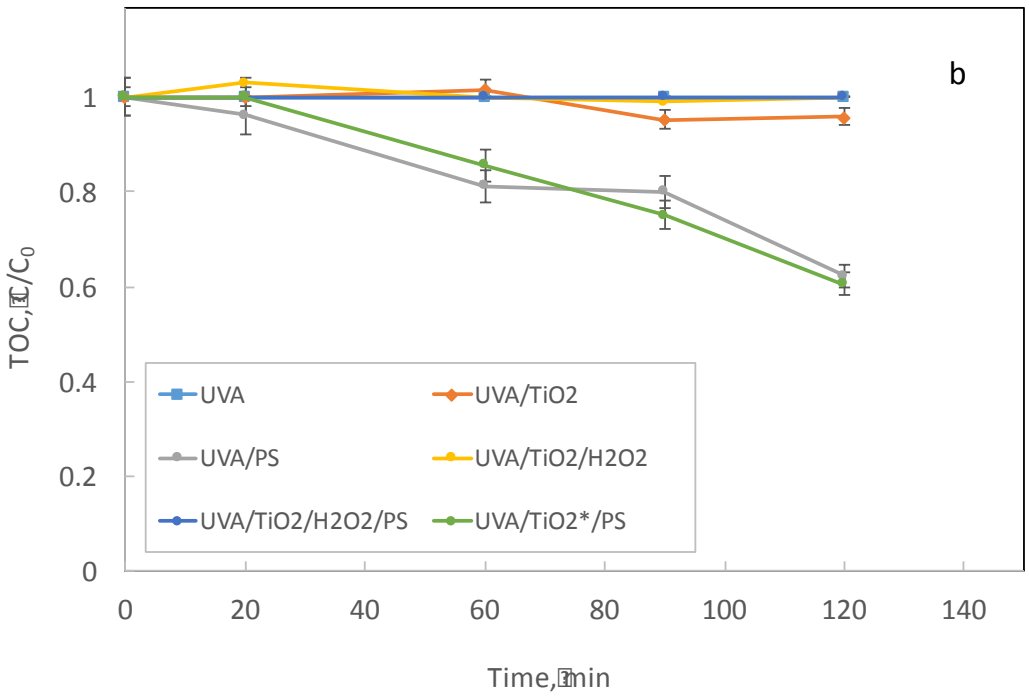

289

290 **Figure 5. Degradation (a) and mineralization (b) of FTD under individual and**

291 **combined heterogeneous processes. Conditions: [TiO_2]=0.37 mg/cm^2, [TiO_2*] = 0.64**

292 **mg/cm^2; [PS]= 2mM.**

This fact changes the degradation pathway, as obtained by LC/MS analysis (data not shown). In this case, and contrary to the mechanism found for the UVC/PS system, the main intermediates formed were $C_{12}H_{17}N_4O_4$ and $C_{11}H_{14}N_3O_4$, which rapidly decreased to form $C_8H_{15}O_3N_3$ and $C_4H_{10}NO$ and $C_5H_{10}NO$ (route 2 in Figure 4). 5-nitro-2-furaldehyde ($C_5H_3O_4N$) is found in a very low concentration.

ii) **Study of cycles/regeneration**

Several cycles re-using the catalyst were carried out to evaluate its possible industrial viability. The results (shown in Figure S6) confirm that degradation is not altered but there is a loss of efficiency (27%) in the mineralization process after 5 cycles of 120 minutes each. However, after regeneration at 500 ºC for two hours, the catalyst recovers its initial performance, even slightly improving efficiency probably due to pore cleansing.

Figure S6, Supplementary Material

3.2.3. Solar process (UVA/TiO_2/PS)

Finally, a new experiment was made under concentrated solar radiation (medium solar power = 38 W/m^2; temperature = 25-36 ºC) using a CPC reactor (described in section 2.3.3) with TiO_2 (0.25 g/L) suspended in water. Results (Figure S7) show that the Solar/TiO_2/PS process has excellent performance during mineralization, comparable with the UVC/PS system.

Figure S7, Supplementary Material

To go deeper into this statement, the stoichiometric efficiency (δ) of PS for TOC degradation was evaluated using the following equation (Fang et al., 2021):

$$\delta = \frac{\Delta_{TOC}}{\Delta_{PS}} \quad (9)$$

where ΔC_{TOC} and ΔC_{PS} represent the degraded TOC and the corresponding consumed PS at the same time, respectively.

In this way, the stoichiometric efficiencies of the more effective processes in terms of TOC degradation (UVC/PS and Solar/TiO_2/PS) have been calculated at the maximum mineralization degree and are resumed in Table 2. The results show that the Solar process has the highest δ value (0.035) after 26 minutes of reaction, which is approximately 1.5 higher that the value obtained for the UVC/PS system after 30 minutes.

Table 2. Stoichiometric efficicency of PS for TOC degradation in selected process for the maximum degradation degree.

Process	Reaction time (min)	Mineralization (%)	Stoichiometric efficiency (δ)
UVC/PS	30	80	0.023
Solar/TiO_2/PS	26	88	0.035

The enhanced stoichiometric efficiency of PS for generating reaction radicals (probably influenced by higher temperature) can explain the best results obtained for this process.

Finally, the evolution of toxicity for the selected Solar/TiO_2/PS process (Figure S8) shows an initial increase due to formation of intermediates, and a later decrease when TOC is reduced. It was confirmed in previous tests that addition of 500 ppm of PS to water increases toxicity in just 0.14 equitox/m^3 while the presence of H_2O_2 in solution is a main contributor to toxicity.

Figure S8, Supplementary Material

At the end of the processes, there is an increase in toxicity probably due to the formation of small amounts of H_2O_2 through reaction of water with the remaining persulfate in solution:

$$S_2O_8^{-2} + 2H_2O \rightarrow 2HSO_4^- + H_2O_2 \quad (10)$$

Although the solar process has to be optimized in future works using real water and including the effect of water matrix, an initial economic study of operation costs comparing different reaction systems has been performed and is resumed in the following section.

3.3. Preliminary economic study of selected processes: operation costs

The processes selected for this study were: UVC/PS in the batch reactor, UVA/TiO_2^*/PS in the thin film reactor and Solar/TiO_2/PS in the CPC. The operation costs that have been considered in the economic study are related to electrical energy and chemicals (reagents and catalysts) consumption. Other costs, such as maintenance have not been considered. A summary of the different operation variables range for each process ie shown in Table S1. The prices of materials (reagents and catalyst) and the electrical consumption of the different devices used for calculating the costs are shown in Table S2. The economic analysis was carried out by analyzing the mineralization process (degradation of total organic carbon present in wastewater).

Tables S1, S2, Supplementary Material

Figure 6a shows the overall (reagents and electricity) operation costs (€/g TOC removed) vs time for the selected processes. It can be seen that the Solar/TiO_2/PS process has lower operation costs due to the use of solar energy instead of artificial UV light. However, it

must be remarked that the solar process would need an additional stage to recover the suspended catalyst from the water before its disposal. This operation has not been considered in this preliminary study and would obviously increase costs in an industrial application.

On the other hand, Figure 6b shows the operation costs (€/g TOC removed), for the three processes as a function of the percentage of TOC removed for the highest mineralization degree reached in each case. The percentage contribution of electricity to the overall operation cost is remarkable in any case. Thus, operation costs can be reduced significantly if the installation is provided with photovoltaic panels and thermal collectors for an energy-free process (Durán et al.,2018).

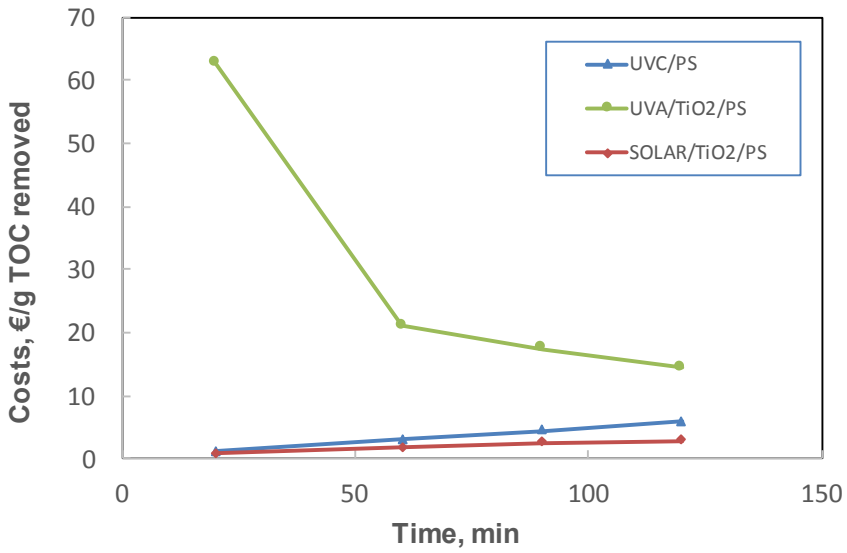

a)

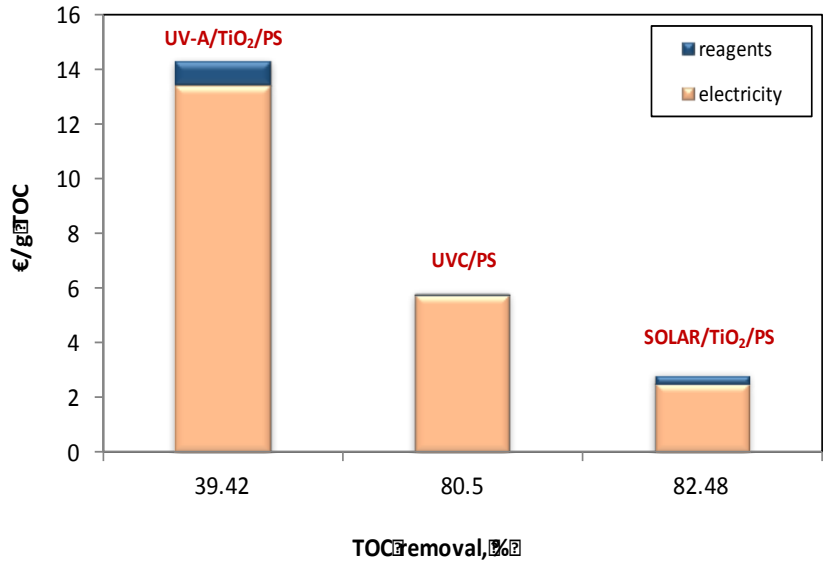

b)

Figure 6. Operation costs for the three selected processes. a) Overall operation costs for the three selected processes. b) Contribution of reagents and electricity as a function of TOC removal for the selected process.

4. Conclusions

- Homogeneous phase:
  - i) Batch reactor: UVC alone produces a slow mineralization ($k = 0.0013\ min^{-1}$). The combined processes are faster ($k_{UVC/H2O2} = 0.0185\ min^{-1}$, $k_{UVC/PS} = 0.0206\ min^{-1}$) with the best performance for the UVC/PS system yielding nearly 80% of mineralization in half an hour. The overall process (UVC/H_2O_2/PS) does not show synergy and mineralization is even slower ($k_{UV/H2O2/PS} = 0.015\ min^{-1}$) due to the production of a high amount of radicals that favours unproductive reactions (scavenger effect). A mineralization mechanism based on sulfate radicals attack is proposed involving the formation of 5hydroxymethylene-2(5H)-furanone and NO as the main intermediates.
- Heterogeneous phase (UVA/TiO_2/PS):
  - i) Batch reactor: the holes play an important role in changing the mineralization mechanism. The main intermediates formed were $C_{12}H_{17}N_4O_4$ and $C_{11}H_{14}N_3O_4$, which rapidly decreased to form $C_8H_{15}O_3N_3$ and $C_4H_{10}NO$ and $C_5H_{10}NO$.
  - ii) The Solar/TiO_2/PS process ([TiO_2] = 0.25 g/L; [PS]= 2mM) has an excellent performance during mineralization, comparable with the UVC/PS system (88 % of TOC removal in 26 min)
- An economic study of operation costs has been made on three selected processes: UVC/PS, UVA/TiO_2/PS and Solar/TiO_2/PS. Electricity is the main contributor to the overall operation cost in all the systems, so that the possible use of photovoltaic panels for an energy process is an interesting option to be considered. The Solar/TiO_2/PS process has the lower operation costs due to the use of solar

energy instead of artificial UV light. However, the solar process would need an additional stage (not considered here) to recover the suspended catalyst from water, increasing costs if used in an industrial application.

Acknowledgement

This work was supported by UCLM-Ayuda a Grupos (2019-GRIN-26900).

References

- Anipsitakis, G.P., Dionysiou, D.D., 2004. Radical Generation by the Interaction of Transition Metals with Common Oxidants. Environ. Sci. Technol. 38, 3705-3712. https://doi.org/10.1021/es035121o
- Awfa, D., Ateia, M.m Fuji, M., Johnson, M.S., Yoshimura, C., 2018. Photodegradation of pharmaceuticals and personal care products in water treatment using carbonaceous-TiO_2 composites: A critical review of recent literature. Wat. Res., 142, 26-45
- Balamurugan, K., Rajakumaran, R., Chen, S.M., Karthil, R., Shim. J.J., Shafi, P.M. 2021. Massive engineering of spinel cobalt tin oxide/tin oxide-based electrocatalyst for the selective voltammetric determination of antibiotic drug furaltadone in water samples. J. Allo y&Comp., 882, 160750.
- Bao, N., Sun, J., Wei, Z.T., Ma, D., Liu, F., Wang, J., 2008. Degradation of biorefractory furaltadone in aqueous solution by ozonation. J. Chem. Technol. Biotechnol. 83, 1347–1352
- Bao, Y., Li, F., Chen, L., Mu, Q., Huang, B., Wen, D. 2021. Fate of antibiotics in engineered wastewater systems and receiving water environment: A case study on the coast of Hangzhou Bay, China. Sci. Tot. Environ. 769, 15 number 144642 https://doi.org/10.1016/j.scitotenv.2020.144642
- Bekkouche, S. Merouani, S., Hamdaoui, Q. Bouhelassa, Q., 2017. Efficient photocatalytic degradation of Safranin O by integrating solar-UV/TiO_2/persulfate treatment: Implication of sulfate radical in the oxidation process and effect of various water matrix components. J. Photochem. Photobiol. A: Chem. 345, 80-91. https://doi.org/10.1016/j.jphotochem.2017.05.028

- Boiarkina, I., Norris, S., Patterson, D.A., 2013. Investigation into the effect of flow structure on the photocatalytic degradation of methylene blue and dehydroabietic acid in a spinning disc reactor, Chem. Eng. J. 222, 159–171.
- Chu, P.S., Lopez, M.I., 2007. Determination of nitrofuran residues in milk of dairy cows using liquid chromatography-tandem mass spectrometry. Journal of Agricultural and Food Chemistry 55, 2129-2135.
- Domínguez, S., Ribao, P., Rivero, M.J., Ortiz, I., 2015. Influence of radiation and TiO_2 concentration on the hydroxyl radicals generation in a photocatalytic LED reactor. Application to dodecylbenzenesulfonate degradation. Appl. Catal. B Environ. 178, 165-169. https://doi.org/10.1016/j.apcatb.2014.09.072
- Dominguez, S., Ribao, P., Rivero, M.J., Ortiz, I., 2015. Influence of radiation and TiO_2 concentration on the hydroxyl radicals generation in a photocatalytic LED reactor. Application to dodecylbenzenesulfonate degradation, Appl. Catal. B Environ. 178, 165–169.
- Durán, A., Monteagudo, J.M., San Martín, 2018. Operation costs of the solar photo-catalytic degradation of pharmaceuticals in water: A mini-review. Chemosphere, 211, 482-488.
- Edhlund, B.L., Arnold, W.A., McNeill, K., 2006. Aquatic photochemistry of nitrofuran antibiotics. Environ. Sci. Technol. 5422-5427.
- Fang, L., Liu, K., Fangbai, L., Zeng, W., Hong, Z., Xu, L., Shi, Q., Ma, Y. 2021. New insights into stoichiometric efficiency and synergistic mechanism of persulfate activation by zero-valent bimetal (iron/cooper) for organic pollutant degradation. J. Hazar. Mater. 403, 123669, 2021

- Farouk, H.U., Raman, A.A.A., Daud, W.M.A.W., 2016. TiO_2 catalyst deactivation in textile wastewater treatment: Current challenges and future advances, J. Ind. Eng. Chem. 33, 11–21.
- Finzi JK, Donato JL, Sucupira M, De Nucci G., 2005, Determination of nitrofuran metabolites in poultry muscle and eggs by liquid chromatography-tandem mass spectrometry, J. Chromatogr. B Analyt Technol Biomed Life Sci. 25;824(1-2):30-5.
- Hu, X.Z., Xu, Y., Yediler, A., 2007. Determinations of residual furazolidone and its metabolite, 3-amino-2-oxazolidinone (AOZ), in fish feeds by HPLC-UV and LC-MS/MS, respectively. Journal of Agricultural and Food Chemistry 55, 1144-1149.
- Kanan, S., Moyet, M.A., Arthur, R.B., Patterson, H.H., 2019. Recent advances on TiO_2 -based photocatalysts toward the degradation of pesticides and major organic pollutants from water bodies. Catalysis Reviews - Science and Engineering, https://doi.org/10.1080/01614940.2019.1613323
- Ibadurrohman, M., Hellgardt, K., 2014. Photoelectrochemical performance of graphene-modified TiO_2 photoanodes in the presence of glycerol as a hole scavenger. Int. J. Hydrogen Ener. 39, 18204-18215.
- Jiménez-Tototzintle, M., Oller, I., Hernández-Ramirez, A., Malato, S., Maldonado, M.I., 2015. Remediation of agro-food industry effluents by biotreatment combined with supported TiO_2/H_2O_2 solar photocatalysis. Chem. Eng. J. 273, 205-215. https://doi.org/10.1016/j.cej.2015.03.060
- Khan, J.A., He, X., Shah, N.S., Khan, H.M., Hapeshi, E., Fatta-Kassinos, D., Dioysiou, D.D., 2014. Kinetic and mechanism investigation on the photochemical degradation of atrazine with activated H_2O_2, $S_2O_8^{-2}$ and HSO_5^-, Chem. Eng. J. 252, 393-403.

- Kumar, M., Jaiswal., S., Sodhi, K.K., Shree, P., Singh, D.K., Agrawal, P.K., Shukla, P., 2019. Antibiotics bioremediation: Perspectives on its ecotoxicity and resistance. Environ. Int. 124, 448-461
- Liang, C. Huang, C.F., Mohanty, N., Kurakalva, R.M., 2008. A rapid spectrophotometric determination of persulfate anion in ISCO. Chemosphere, 73 1540-1543
- Marques-Violante, F.G., Oliveira-Rosas, C., Freitas-Guimarães, E., Carvalho-Vital, H., Oliveira-Cavalcanti, N., Radler-Aquino, F., 2018. Feasibility study for the development of a certified reference material of nitrofuran metabolites in chicken breast muscle from incurred samples. Measurement, 129, 368-374
- Matta, R. Tlili, S. Chiron, S. Barbati, S., 2011, Removal of carbamazepine from urban wastewater by sulfate radical oxidation. Environ. Chem. Lett. 9, 347-353. https://doi.org/10.1007/s10311-010-0285-z
- Mills, A., Valenzuela, M.A., 2004. The photo-oxidation of water by sodium persulfate, and other electron acceptors, sensitized by TiO_2. J. Photochem. Photobiol. A: Chem. 165 (2004) 25-34. https://doi.org/10.1016/j.jphotochem.2004.02.017
- Monteagudo, J.M., Durán, A., Latorre, J., Expósito, A.J., 2016. Application of activated persulfate for removal of intermediates from antipyrine wastewater degradation refractory towards hydroxyl radical. J. Hazard. Mater. 306, 77-86
- Monteagudo, J.M., Durán, San Martín, Aguitrre, M., 2010. Effect of light source on the catalytic degradation of protocatechuic acid in a ferrioxalate-assisted photo-Fenton process. Appl. Catal B: Env., 96, 486-495.
- Monteagudo, J.M., Durán, A., Martínez, M.R., San Martín, I. Effect of reduced graphene oxide load into TiO2 P25 on the generation of reactive oxygen species in a

solar photocatalytic reactor. Application to antipyrine degradation (2020) Chem Eng. J, 380, 122410

- Monteagudo, J.M., Durán, San Martín, I., Vellón, B. 2020b. Photocatalytic degradation of aniline by solar/TiO_2 system in the presence of the electron acceptors $Na_2S_2O_8$ and H_2O_2. Sep. Pur. Technol. 238, 116456. https://doi.org/10.1016/j.seppur.2019.116456
- Nakamura, H., Kawakami, T., Niino, T., Takahashi, Y., Onodera, S., 2008. Chemical fate and changes in mutagenic activity of antibiotics nitrofurazone and furazolidone during aqueous chlorination. The Journal of Toxicological Sciences 33, 621-629.
- Norzaee, S., Bazrafshan, E., Djahed, B., Mostafapour, F.K., Khaksefidi, R., 2017. UV Activation of Persulfate for Removal of Penicillin G Antibiotics in Aqueous Solution, The Sci. World Journal, Article ID 3519487. https://doi.org/10.1155/2017/3519487
- Pacholak, A., Zdarta, A., Frankowski, R., Cybulski, Z., Kaczorek, E. 2020. Exploring Elimination Kinetics of Four 5-Nitrofuran Derivatives by Microbes Present in Rural and Municipal Activated Sludge. Water Air Soil Pollut (2020) 231: 252 https://doi.org/10.1007/s11270-020-04634-7
- Saien, J., Ojaghloo, Z., Soleymani, A.R., Rasoulifard, M.H., 2011. Homogeneous and heterogeneous AOPs for rapid degradation of Triton X-100 in aqueous media via UV light, nano titania hydrogen peroxide and potassium persulfate. Chem. Eng. J. 167, 172-182. https://doi.org/10.1016/j.cej.2010.12.017
- Samuelsen, O.B., Solheim, E., Lunestad, B.T., 1991. Fate and microbiologial effects of furazolidone in a marine aquacultural sediment. The Science of The Total Environment 108, 275-283.

- Van Grieken, R., Marugán, J., Sordo, C. Pablos, C., 2009. Comparison of the photocatalytic disinfection of E. coli suspensions in slurry, wall and fixed-bed reactors. Catal. Today 144, 48-54.
- Yu, C.H. Wu, C.H., Ho, T.H., Andy-Hong, P.K., 2010. Decolorization of C.I. Reactive Black 5 in UV/TiO2, UV/oxidant and UV/TiO_2/oxidant systems: A comparative study. Chem. Eng. J. 158, 578-583. https://doi.org/10.1016/j.cej.2010.02.001
- Yu, W.H., Chin, T.S., Lai, H.T., 2013. Detection of nitrofurans and their metabolites in pond water and sediments by liquid chromatography (LC)-photodiode array detection and LC-ion spray tandem mass spectrometry. International Biodeterioration & Biodegradation 85, 517-526.

SUPPLEMENTARY MATERIAL

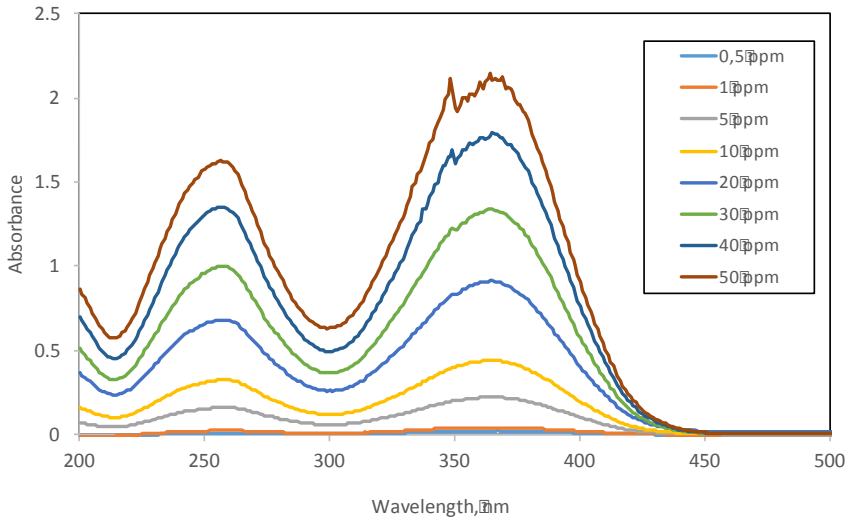

Figure S1. Absorption spectra of Furaltadone

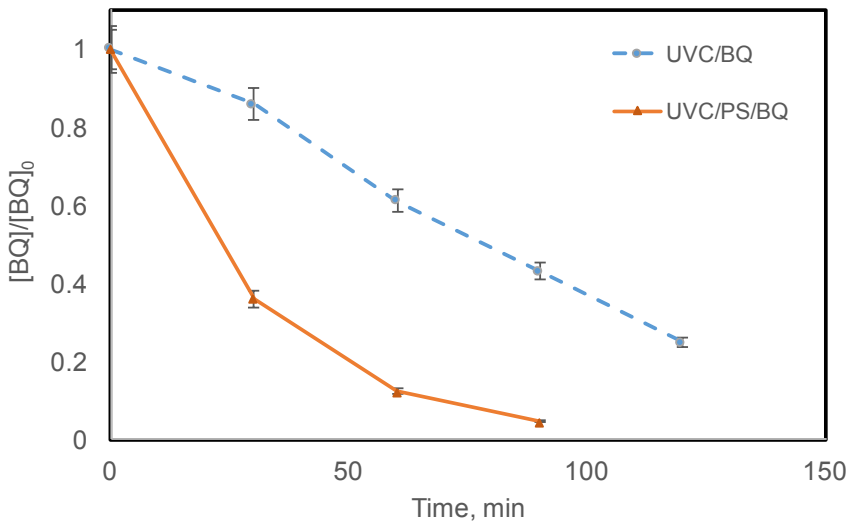

Figure S2. Evolution of BQ concentration in the presence of PS and UVC light:

(Conditions: [PS] = 500 mg/L, [BQ] = 2 mM).

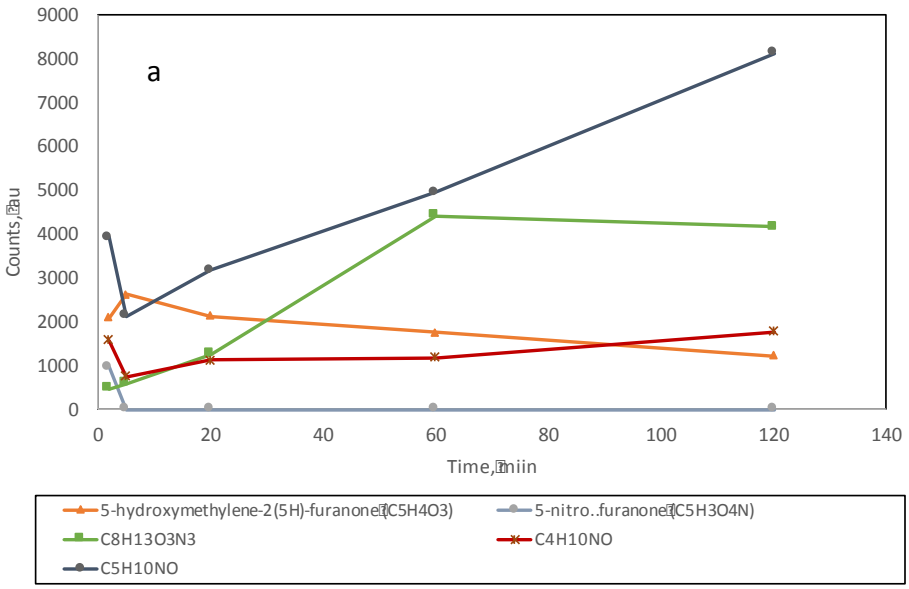

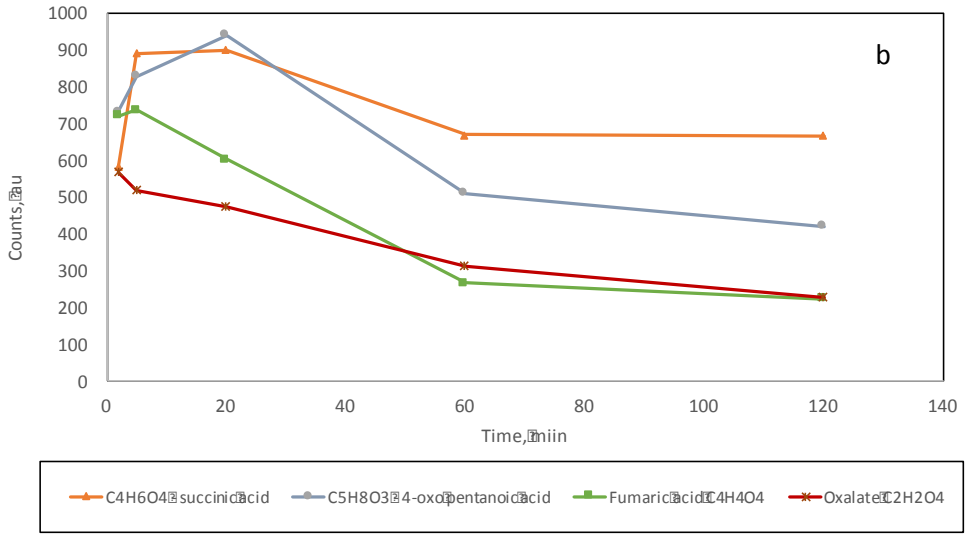

Figure S3. Intermediate products detected by LC-MS in a) positive mode; b) negative mode. Process: UVC/PS. Conditions: T = 30ºC, pH = 3.5, [PS]= 2 mM; [FTD]= 0.03 mM.

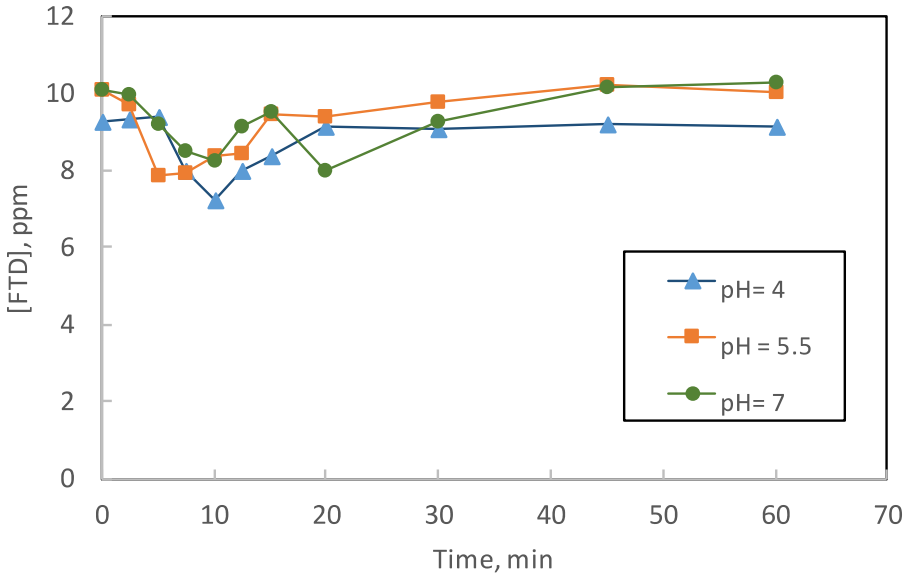

Figure S4. Adsorption of Furaltadone with TiO_2 at different pHs. ([TiO_2]= 0.5 g/L)

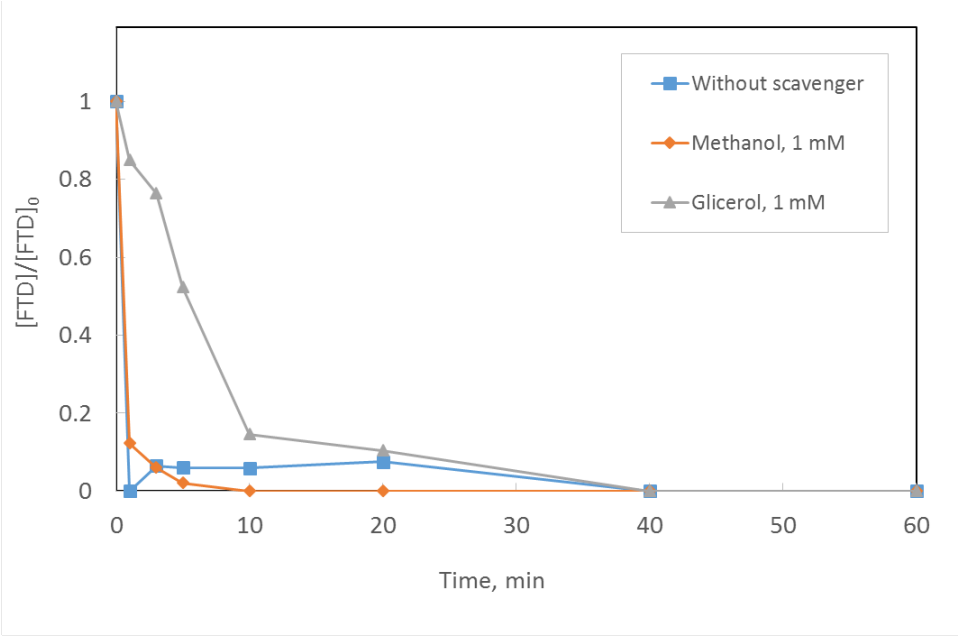

Figure S5. Degradation of FTD under the effect of different scavenger agents in the UVA/TiO_2/ PS process. (Conditions: [FTD] = 0.03 mM; T = 30ºC; [PS]= 2 mM; [TiO_2]= 0.64 mg/cm^2)

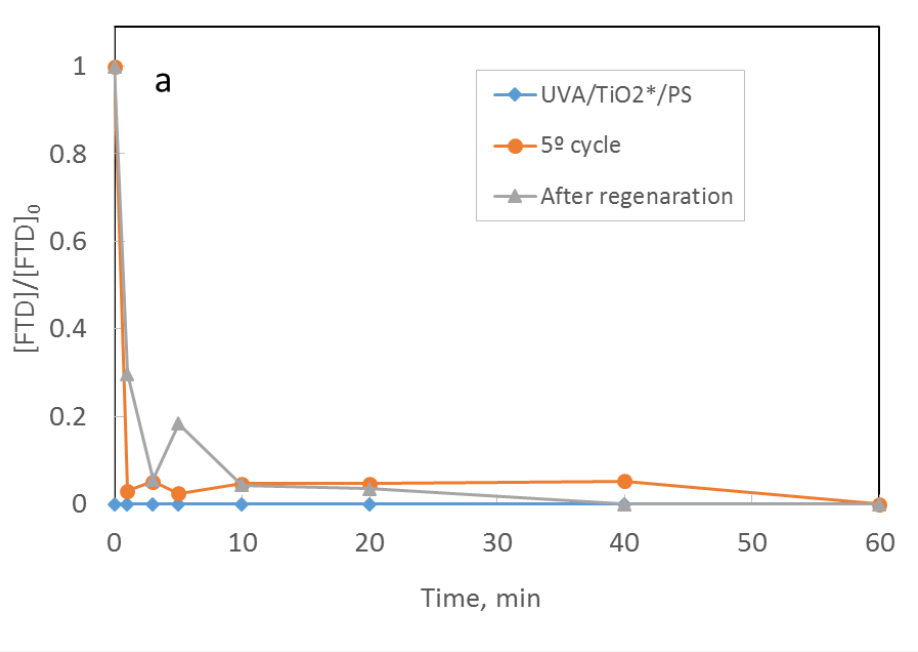

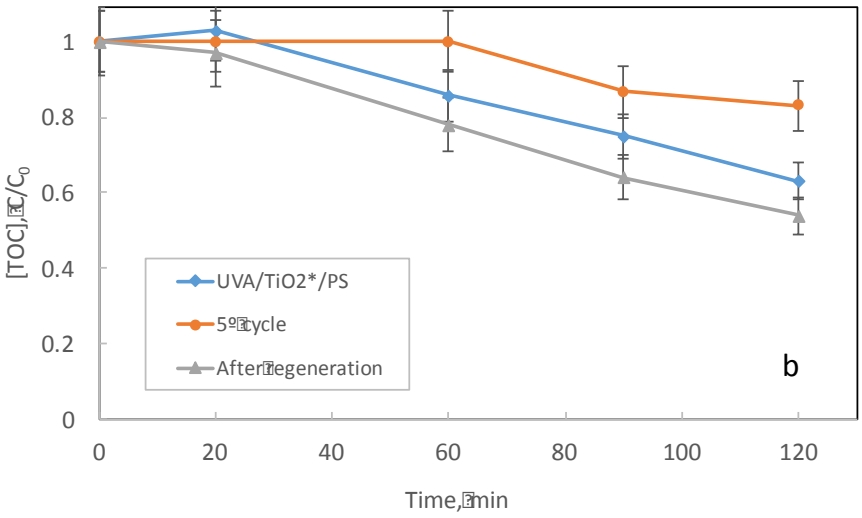

Figure S6. Re-use of the catalyst after 5 cycles in the UVA/TiO_2/PS process. a) Effect on FTD degradation; b) Effect on TOC removal. (Conditions: [FTD] = 0.03 mM; T = 30ºC; [PS]= 2 mM; [TiO_2]= 0.64 mg/cm^2)

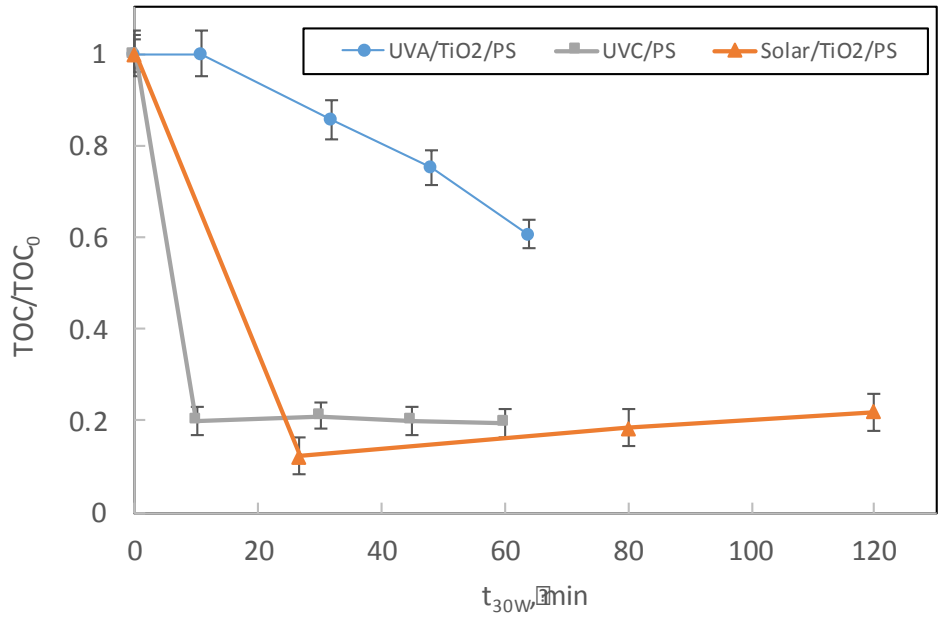

Figure S7. Comparison of performance of different processes. Common Conditions: [FTD] = 0.03 mM; [PS]= 2 mM; T = 30°C. Catalyst concentration: UVA/TiO_2*/PS: [TiO_2]= 0.64 mg/cm^2; Solar/TiO_2/PS: [TiO_2]= 0.25 g/L;

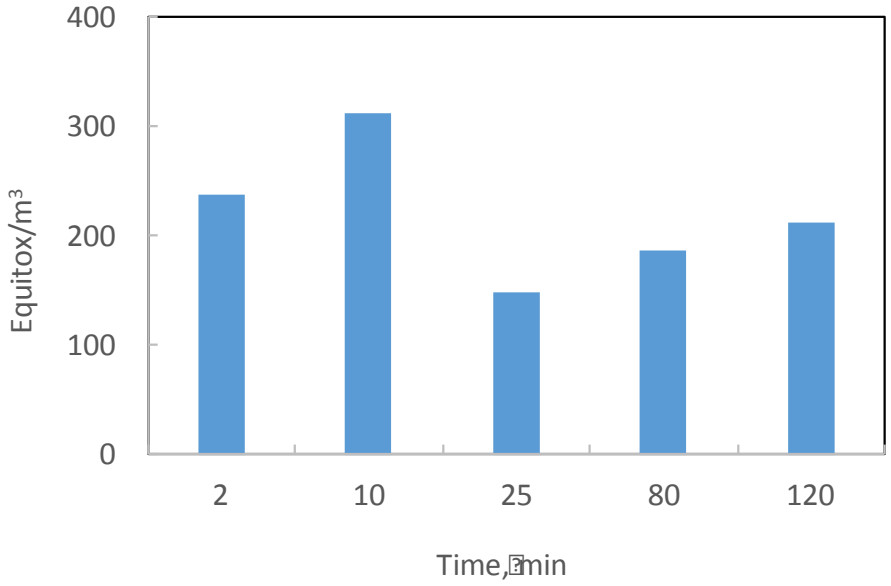

Figure S8. Evolution of toxicity during the solar/TiO_2/PS process.

Table S1. Technical conditions for the photocatalytic processes selected for the economic study

Process	Experimental device	Optimum operating conditions	Maximum mineralization degree
UVC/PS	UVC lab reactor of 0.4 L with a 15 W UVC lamp (254 nm)	[PS] = 2 mM pH = 4 Temperature = 30 ºC	79.1% in 20 min
UVA/TiO_2/PS	Thin film reactor of 0.4 L 2x8 W UVA lamps (> 350 nm).	[TiO_2] = 0.64 mg/cm^2 [PS] = 2 mM pH = 4 Temperature = 30 ºC	39.5% in 64 min
Solar/TiO_2/PS	CPC solar reactor (2.5 L), with a solar collector area of 0.25 m^2. The total illuminated volume is 2 L	[TiO_2] = 0.25 g/L [PS] = 2 mM pH = 4 Temperature = 25-36 ºC	78 % in 26 min

Table S2. Electric power and costs of electricity and reagents

ELECTRIC POWER	
UVC reactor	
Lamp	0.0236 kW
Stirrer	0.0250 kW
pH-meter	0.0066 kW
UVA reactor	
Lamp	0.0175 kW
Stirrer	0.0250 kW
pH-meter	0.0066 kW
Solar CPC reactor	
Pump, pH meter, etc.	0.200 kW
ENERGY COST (industrial rate) [UNESA. 2015]	
0.0912 €/kWh	
REAGENTS COSTS	
TiO_2	0.0052 €/g
Sodium persulfate	0.71 €/kg
Sulfuric acid	0.183 €/L

Text S1: LC/MS analysis:

The QTOF-UHPLC analysis was conducted using a MaXis HD quadrupole electrospray time-of-flight (ESI-QTOF) mass spectrometer (Bruker Daltonik GmbH, Bremen, Germany), which was coupled to an Ultimate 3000 UHPLC (Thermo Fisher Scientific, California, USA) for infusions. Analyses were performed in both ESI positive and negative-ion modes. The capillary voltage was set to 4500 V, nebulizing gas at 1 bar, drying gas at 7 L/min at 200°C in each case. The TOF scan range was 50 – 1000 mass-to-charge ratio (*m/z*). Infusion injections of 100 µL were performed by the autosampler using a flow rate set to inject speed of 240 µL/min in conjunction with 80 µL/min MeOH with 0.1% FA flow from the pump. The MS instrument was calibrated every 5 injections using a similar 10 µL injection of sodium formate calibrant solution. The calibrant solution consisted of 3 parts of 1 M NaOH to 97 parts of 50:50 water:isopropanol with 2% formic acid. The observed mass and isotope pattern matched the corresponding theoretical values calculated from the expected elemental formula within 2 ppm mass accuracy. Mass features were detected as $[M + H]^+$, $[M - H]^-$ or $[M + Cl]^-$ ions with within 0.005 Da. The averaged mass spectra between 1.0 - 2.0 min were used to determine the peak counts. Data processing was performed using the Compass Data Analysis software version 4.3 (Bruker Daltonik GmbH, Bremen, Germany).

Text S2. Dip- coating method

The glass plate was first cleaned with soap and water and then immersed in a KOH–isopropanol bath (200 g L^{-1}) for 24 h. It is later rinsed with water to remove the isopropanol, followed by ultrasonication for 20–30 min. A mixture of TiO_2 and deionized water (150-300 g L^{-1} in deionized water at a pH of 1.5) The process was assisted by a Bungard Elektronik RDC- 15 equipment working at a controlled withdrawal speed of 0.65 mm s^{-1}. Finally, the plate was dried at 110 °C for 24 h and calcined at 500 °C for 2 h at the heating rate of 5 °C min^{-1}. The process was repeated several times to obtain different catalyst loadings.